LETTER

https://doi.org/10.1038/s41586-019-1145-z

# High-temperature bulk metallic glasses developed by combinatorial methods

Ming-Xing Li[1,2], Shao-Fan Zhao[3], Zhen Lu[4], Akihiko Hirata[4], Ping Wen[1,2], Hai-Yang Bai[1,2,5], MingWei Chen[4,6], Jan Schroers[3], YanHui Liu[1,2,5,7]* & Wei-Hua Wang[1,2,5,7]

**Since their discovery in 1960[1], metallic glasses based on a wide range of elements have been developed[2]. However, the theoretical prediction of glass-forming compositions is challenging and the discovery of alloys with specific properties has so far largely been the result of trial and error[3–8]. Bulk metallic glasses can exhibit strength and elasticity surpassing those of conventional structural alloys[9–11], but the mechanical properties of these glasses are critically dependent on the glass transition temperature. At temperatures approaching the glass transition, bulk metallic glasses undergo plastic flow, resulting in a substantial decrease in quasi-static strength. Bulk metallic glasses with glass transition temperatures greater than 1,000 kelvin have been developed, but the supercooled liquid region (between the glass transition and the crystallization temperature) is narrow, resulting in very little thermoplastic formability, which limits their practical applicability. Here we report the design of iridium/nickel/tantalum metallic glasses (and others also containing boron) with a glass transition temperature of up to 1,162 kelvin and a supercooled liquid region of 136 kelvin that is wider than that of most existing metallic glasses[12]. Our Ir–Ni–Ta–(B) glasses exhibit high strength at high temperatures compared to existing alloys: 3.7 gigapascals at 1,000 kelvin[9,13]. Their glass-forming ability is characterized by a critical casting thickness of three millimetres, suggesting that small-scale components for applications at high temperatures or in harsh environments can readily be obtained by thermoplastic forming[14]. To identify alloys of interest, we used a simplified combinatorial approach[6–8] harnessing a previously reported correlation between glass-forming ability and electrical resistivity[15–17]. This method is non-destructive, allowing subsequent testing of a range of physical properties on the same library of samples. The practicality of our design and discovery approach, exemplified by the identification of high-strength, high-temperature bulk metallic glasses, bodes well for enabling the discovery of other glassy alloys with exciting properties.**

The design of Ir–Ni–Ta–(B) high-temperature bulk metallic glasses (BMGs) starts with an Ir–Ta binary system, and is based on established correlations among physical properties and empirical criteria for enhancing their glass-forming ability (GFA). The glass transition temperature $T_g$ of a BMG has been demonstrated to correlate with the elastic modulus $E$ (refs [18,19]) and the melting temperature $T_m$ (ref. [20]) of its constituent elements. Since Ir has a large $E$ (the second-highest among metals, after osmium) and a very high $T_m$, incorporation of Ir into an alloy suggests a similarly high $T_g$. Among Ir binary alloys, Ir–Ta has been reported to form glasses at high cooling rates of $10^8$ K s$^{-1}$ (ref. [21]); Ta has the fourth-highest $T_m$ among the metallic elements. Ni was chosen because it differs in atomic size by more than 12% compared to Ir and Ta and has a large negative heat of mixing with both elements (Fig. 1a), obeying Inoue's empirical criteria for designing BMGs[12]. Furthermore, binary Ni–Ta is a glass-forming system[22], and Ni is completely soluble in Ir. Such characteristics have been recognized to improve the GFA of ternary alloy systems[12,23,24]. To further improve the GFA, we chose B because it has a high melting temperature (2,365 K) and exhibits characteristics associated with enhancing the GFA of Ir–Ni–Ta, such as its small size and large negative heat of mixing compared to the other three elements (Fig. 1a). The thermal stability ($\Delta T = T_x - T_g$)—the difference between the glass transition and crystallization temperatures—of a BMG is related to its GFA[12,23]. Therefore, we begin our search for BMGs with high $T_g$ and large $\Delta T$ in the Ir–Ni–Ta–(B) system by looking at specific alloys with a high GFA, especially alloys rich in Ir and Ta.

We first focus on ternary Ir–Ni–Ta alloys because the compositional space of a ternary system is two orders of magnitude smaller than a quaternary system[3]. In the past, a starting point for identifying BMG-forming alloys was to search for deep eutectic compositions where the liquid is stable and crystallization is possible only at lower temperatures[12,23]. As other aspects also control glass formation, such as interfacial energy and compositional difference between liquid and solid, the alloy with the best GFA does not always have the same composition as the deep eutectics[5]. In the isothermal projection of the ternary Ir–Ni–Ta phase diagram[25], eutectics exist and cover a wide composition range (Fig. 1b). If one atomic per cent in one constituent is taken as the interval by which to distinguish two alloys[3], the number of alloys covered by the eutectic points substantially exceeds those that can be considered with a traditional trial-and-error approach for BMG development. Furthermore, locating eutectics relies on phase diagrams. Although the diagrams can be easily found for simple binary alloy systems and few ternary systems, they are not usually available for multiple-component alloy systems. Hence, to discover alloys that exhibit high GFA, we performed massive parallel synthesis paired with high-throughput characterizations.

Specifically, we simultaneously fabricated a large compositional library through magnetron co-sputtering, a technique which has been used in many different fields, including the fabrication of metallic glasses[6–8] (Fig. 1c). The desired alloy range of the compositional libraries is achieved by altering the orientation angles of the sputtering targets relative to the substrate, and by tuning the sputtering power applied to the targets[7] (Fig. 1c). As shown in Fig. 1c and d, the libraries were deposited on silicon substrates 100 mm in diameter from targets made of single elements. We fabricated libraries of different compositional gradients, covering nearly the entire ternary phase diagram, such as 0–90% Ir, 0–90% Ni and 10–100% Ta (Fig. 2a). X-ray diffraction (XRD) mapping revealed that approximately 50% of the considered alloys in the Ir–Ni–Ta system form a glass phase (Fig. 2a) owing to the high cooling rate of sputtering[26], which cover 10–50% Ir, 0–70% Ni, and 30–85% Ta. Such a broad glass-forming composition range suggests that potential glass-forming alloys may be overlooked because only a few discrete compositions are typically attempted when using the conventional trial-and-error alloy development method.

For high-throughput characterization, we consider electrical resistivity measurements. It has been suggested that the electronic structure of

[1]Institute of Physics, Chinese Academy of Sciences, Beijing, China. [2]University of Chinese Academy of Sciences, Beijing, China. [3]Department of Mechanical Engineering and Materials Science, Yale University, New Haven, CT, USA. [4]World Premier International Research Centers Initiative (WPI), Advanced Institute for Materials Research, Tohoku University, Sendai, Japan. [5]Songshan Lake Materials Laboratory, Dongguan, China. [6]Department of Materials Science and Engineering, Johns Hopkins University, Baltimore, MD, USA. [7]Beijing Advanced Innovation Center for Materials Genome Engineering, University of Science and Technology Beijing, Beijing, China. *e-mail: yanhui.liu@iphy.ac.cn

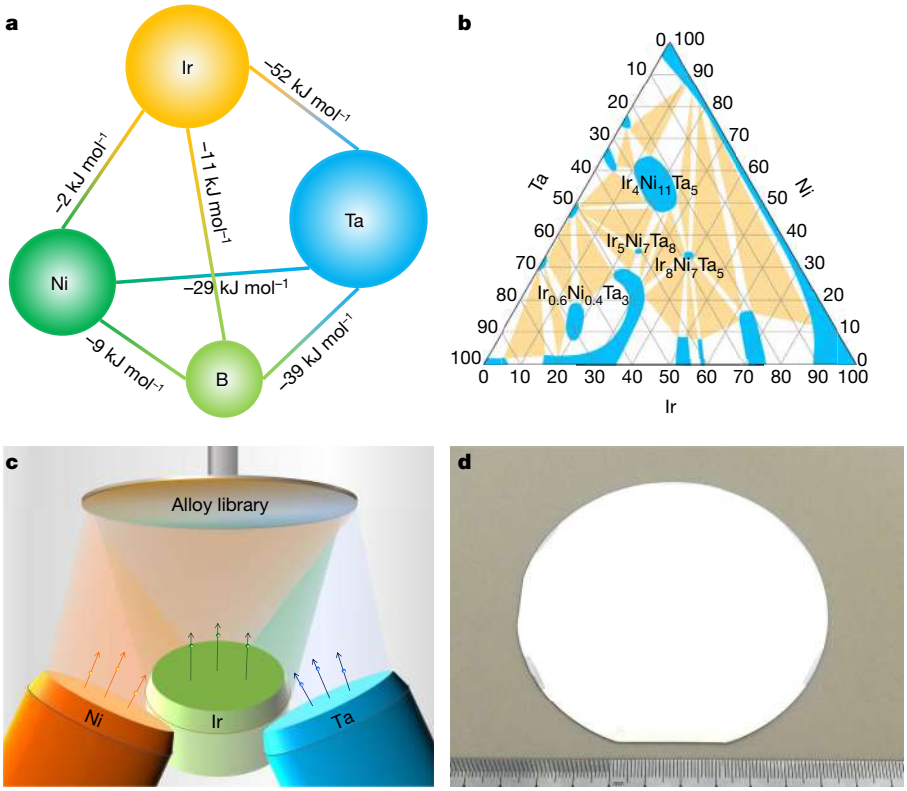


**Fig. 1 | Design and combinatorial fabrication of Ir–Ni–Ta–(B) bulk metallic glass forming alloy system. a**, The heat of mixing between the selected elements is shown and their relative size difference is indicated by spheres. **b**, Isothermal projection of the Ir–Ni–Ta ternary phase diagram. Reprinted with permission from ASM International (all rights reserved; www.asminternational.com)[25]. **c**, A schematic diagram of magnetron co-sputtering. **d**, The appearance of the combinatorial thin-film materials library deposited on a 100-mm-diameter silicon wafer.

an alloy can affect the stability of a glassy structure and that increased stability of the amorphous structure is realized when the Fermi surface touches the quasi-Brillouin boundary[15,16]. Energy gaps are predicted to occur at the boundaries of Brillouin zones, where energy levels are forbidden and the density of energy states is suppressed, leading to the reduced electronic conductivity that is often associated with enhanced GFA[15–17] (see also Methods). To rapidly unveil the composition range in which alloys of high GFA may exist, we take this correlation as a guideline. Figure 2b shows the variation of sheet resistance with composition for as-deposited libraries without any post-deposition processing. As can be seen, in the ternary plot (Fig. 2b), there exists a region of higher electrical resistance, suggesting that alloys within this region may have higher GFA. This argument is supported by the fact that the curved band-like region extends towards the known glass-forming compositions in the binary Ir–Ta and Ni–Ta systems[21,22], as indicated by the two black dots in Figure 2b. Since our aim is to identify BMGs with high $T_g$, we consider alloys that are rich in Ir and Ta within the high-resistance region (see the thin solid line in Fig. 2b), because they have higher $T_m$ and $E$, indicating higher $T_g$ (refs [18–20]). This region is small enough that it can be evaluated by samples prepared through conventional copper-mould suction casting with cooling rates that are orders of magnitude lower than those during sputtering. We found that within the composition range of 20–35% Ir, 35–40% Ta, and 25–40% Ni (see the purple dots in Fig. 2b), 2-mm-diameter fully glassy rods are readily achievable (Fig. 2c), which was confirmed by XRD (Fig. 2d). In the considered composition range, $Ir_{33}Ni_{28}Ta_{39}$ exhibits the highest GFA, as reflected by fully glassy rods of 3 mm diameter (Fig. 2c and d). The critical cooling rate for $Ir_{33}Ni_{28}Ta_{39}$ is estimated to be about 100 K $s^{-1}$, comparable to that for the majority of known BMG-forming alloys[12]. Addition of B further improves GFA. For example, by substituting Ni with 5% B, the critical rod diameter can be increased from 2 mm for $Ir_{35}Ni_{25}Ta_{40}$ to 3 mm for $Ir_{35}Ni_{20}Ta_{40}B_5$ (see Fig. 2c and the XRD spectra of Fig. 2d). Since few impurities in BMG rods and raw materials are detected (Extended Data Table 1), the increased GFA can be attributed to the addition of a minor amount of B. The formation of bulk glasses confirms that mapping electrical resistance is an effective high-throughput approach, and so combinatorial synthesis can be substantially simplified because complicated pre-/post-sputtering procedures[7,8] can be avoided. The approach is translatable to a broad range of alloy systems so that compositions of high GFA can be identified.

The large thermal stability and the extraordinarily high $T_g$ of the Ir–Ni–Ta–(B) alloys can be seen in Fig. 2e. For $Ir_{35}Ni_{25}Ta_{40}$, $T_g$ reaches 1,162 K. To our knowledge, this is the highest $T_g$ reported for a BMG (Fig. 3a). Addition of B slightly reduces $T_g$ to 1,147 K, probably owing to the lower $T_m$ of B, but the increase in $T_x$ to 1,283 K leads to a broadened supercooled liquid region (Figs. 2e and 3a). For $Ir_{35}Ni_{20}Ta_{40}B_5$, $\Delta T$ reaches 136 K, which is among the widest reported supercooled liquid regions for BMGs (Fig. 3a). Except for $Ir_{25}Ni_{35}Ta_{40}$, most of the ternary BMG-forming alloys have compositions that are different from eutectics, exhibiting two melting peaks (Fig. 2f). According to the measured $T_g$, $T_x$ and the liquidus temperature $T_l$, the GFA indexes $T_{rg} = T_g/T_l$ (ref. [27]) and $\gamma = T_x/(T_g + T_l)$ (ref. [28]) are estimated to be 0.65–0.69 and 0.424–0.454 for the Ir–Ni–Ta–(B) alloys. Such $T_{rg}$ and $\gamma$ values are comparable to BMGs of high thermoplastic formability, such as Zr-, Pt- and Au-based glass-forming alloys[14].

The high $T_g$ of the high-temperature BMGs suggests that their strength can be maintained at high temperatures, potentially even beyond 1,000 K. As can be seen in Fig. 3b, the strength of $Ir_{35}Ni_{25}Ta_{40}$ high-temperature BMG is 5.1 GPa at room temperature (approximately 21 °C) and remains as high as 3.7 GPa, even at 1,040 K. Such strength is up to an order of magnitude higher than that of high-temperature alloys and high-entropy alloys at similar temperature[9,13]. The large $\Delta T$ of the high-temperature BMGs (Fig. 3a) implies that they are highly processable in their supercooled liquid region, which can be quantified by $S = (T_x - T_g)/(T_l - T_g)$ (ref. [14]). For $Ir_{35}Ni_{20}Ta_{40}B_5$, the $S$ parameter is estimated to be around 0.255, similar to BMGs with high

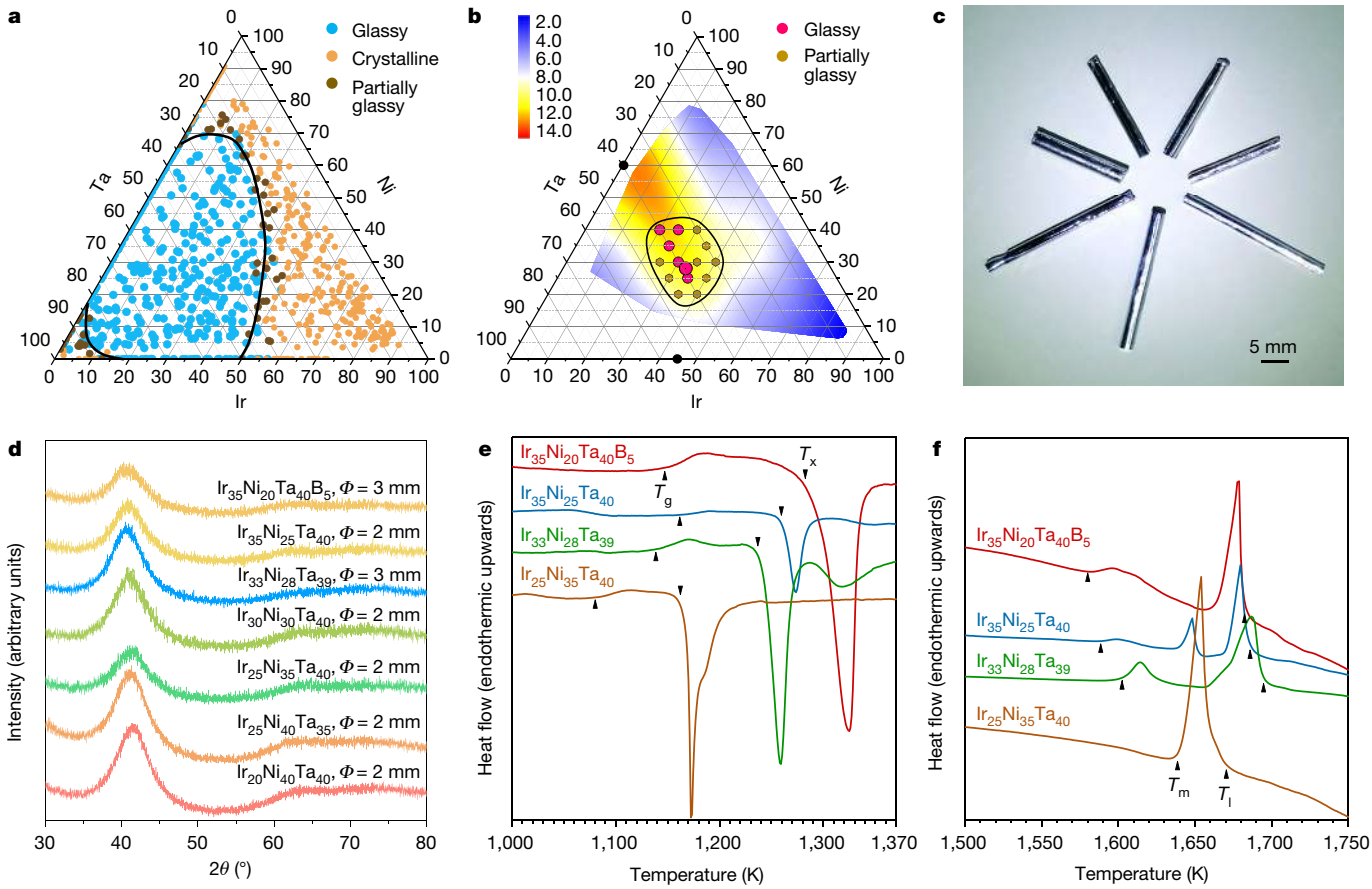


**Fig. 2 | High-throughput characterizations of Ir–Ni–Ta–(B) bulk metallic glasses. a**, The glass-forming range of the Ir–Ni–Ta ternary system under high cooling rate by sputtering. **b**, A square resistance mapping showing the variation of electrical resistivity (in units of ohm per square) with compositions. The yellow region of higher resistance suggests better glass-forming ability. Alloys indicated by pink dots can be cast into glassy rods by copper mould casting. **c**, Appearance of as-cast Ir–Ni–Ta–(B) glassy rods. **d**, X-ray diffraction spectra of bulk rods. $\Phi$, rod diameter. **e**, Glass transition and crystallization behaviours of the BMGs. For each alloy, the arrow pointing upwards indicates the glass transition temperature and the one pointing downwards indicates the crystallization temperature. **f**, Melting behaviour of the Ir–Ni–Ta–(B) alloys. For each alloy, the arrow on the left indicates the melting temperature and the one on the right indicates the liquidus temperature.

thermoplastic formability[14]. To demonstrate the thermoplastic formability of the Ir–Ni–Ta–(B) BMGs directly, we drew micro-wires by thermoplastic forming. As shown in Fig. 4a, an initial 1-mm-diameter rod was drawn into a thin wire of diameter as small as about 45 μm under a force of 1 N for 2 s. Although the high-temperature BMG in the supercooled liquid region is soft and thermoplastically processable, nanoindentation tests reveal a hardness of 15 GPa and a Young's modulus of 263 GPa for $Ir_{35}Ni_{20}Ta_{40}B_5$ at room temperature, which

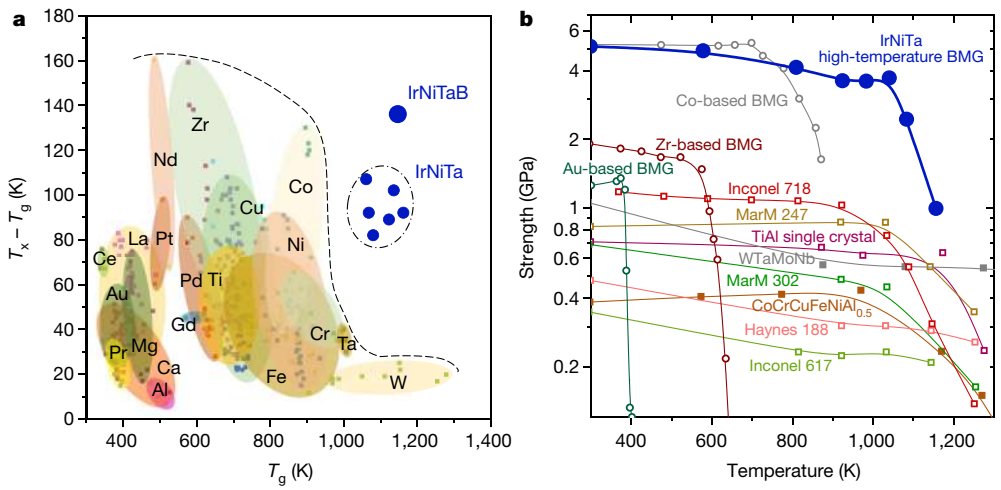


**Fig. 3 | Summary of the supercooled liquid region versus the glass transition temperature and the high temperature strength of various alloys. a**, The supercooled liquid region ($\Delta T = T_x - T_g$) versus $T_g$ for our Ir–Ni–Ta–(B) high-temperature BMGs and typical known BMGs. Only data for glasses that form in bulk are included, except for the W-based alloys, which have marginal glass-forming ability. The vast majority of BMGs have $T_g < 1{,}000$ K and $\Delta T < 100$ K. **b**, Strength versus temperature for our Ir–Ni–Ta high-temperature BMGs as well as a variety of alloy classes including high-temperature alloys, high-entropy alloys and Au-, Zr- and Co-based BMGs[9–13].

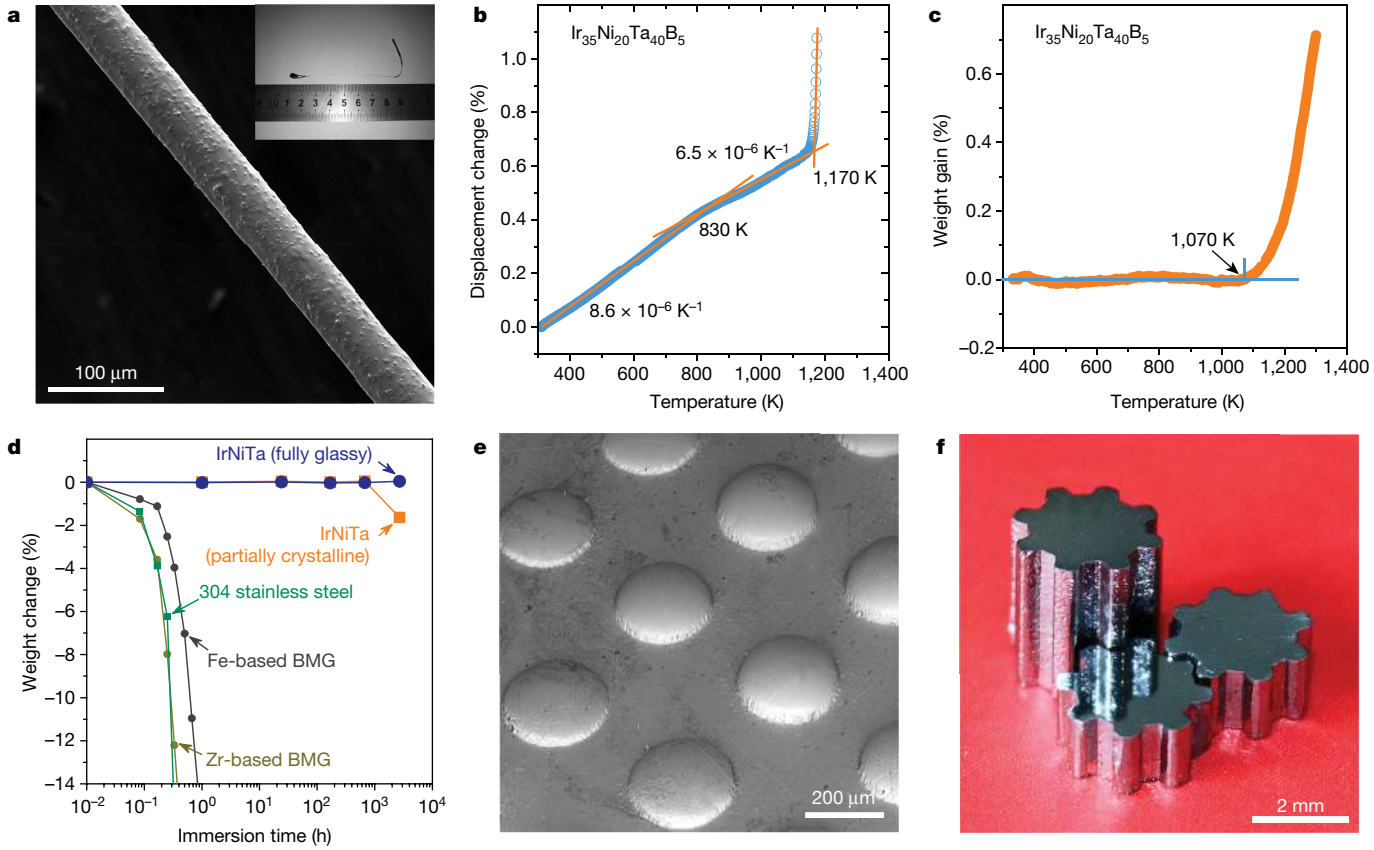


**Fig. 4 | Properties of our Ir–Ni–Ta–(B) BMGs. a**, An $Ir_{35}Ni_{20}Ta_{40}B_5$ micro-wire with diameter around 45 μm processed via thermoplastic forming. **b**, The thermal expansion of $Ir_{35}Ni_{20}Ta_{40}B_5$ BMG in its glass state. **c**, The strong oxidation resistance of $Ir_{35}Ni_{20}Ta_{40}B_5$ BMG up to 1,070 K in air. **d**, In aqua regia, 304 stainless steel and Zr- and Fe-based BMGs are corroded within one hour. However, our fully glassy $Ir_{35}Ni_{25}Ta_{40}$ BMG rod showed no weight loss for up to 112 days. The partially crystalline $Ir_{35}Ni_{25}Ta_{40}$ rod exhibited measurable weight loss after 28 days. **e**, An $Ir_{33}Ni_{28}Ta_{39}$ microscale mould fabricated by thermoplastic forming. **f**, $Ir_{33}Ni_{28}Ta_{39}$ micro-gears fabricated by copper mould casting.

are values unprecedented for BMGs. The bending strain to failure rate of about 2.9% for the as-cast $Ir_{35}Ni_{20}Ta_{40}B_5$ BMG suggests that it has moderate ductility[29] despite high hardness and modulus. The linear thermal expansion coefficient of $Ir_{35}Ni_{20}Ta_{40}B_5$ high-temperature BMG was measured to be $8.6 \times 10^{-6}\,K^{-1}$ at temperatures lower than 830 K, and $6.5 \times 10^{-6}\,K^{-1}$ for temperatures above 830 K (Fig. 4b). Compared to published data on BMGs[30], such thermal expansion coefficients are among the smallest values.

Figure 4c shows the oxidation behaviour of $Ir_{35}Ni_{20}Ta_{40}B_5$ high-temperature BMG as a function of temperature measured in air. No substantial weight change can be observed up to 1,070 K, a temperature close to its $T_g$. Annealing tests further confirm that the high-temperature BMGs can be exposed to high temperatures in air without substantial oxidation (Extended Data Figs. 1, 2). Oxidation resistance is often associated with general resistance to corrosion. As shown in Fig. 4d, corrosion takes place within an hour in 304 stainless steel, and in Zr- and Fe-based BMGs when they are immersed in aqua regia. However, no weight loss in the fully glassy IrNiTa high-temperature BMG can be seen even after 112 days, while the partially crystalline IrNiTa sample exhibits obvious weight loss after 28 days. This finding reveals that the high-temperature BMGs can withstand extremely corrosive conditions. It also highlights the importance of both chemistry and microstructure for the corrosion resistance as the partially crystalline alloy reacts much faster.

The combination of superb properties and plastic-like processability—wide $\Delta T$ and high GFA, high-temperature strength, excellent thermoplastic formability, low thermal expansion, superior oxidation and corrosion resistance—make the Ir–Ni–Ta–(B) high-temperature BMGs promising for a range of technological applications at low and ambient temperatures but also at temperatures beyond 1,000 K and even in extreme environments. For example, taking advantage of their thermoplastic formability, mechanical properties, and low thermal expansion, the glasses are excellent candidates for fabrication of micro- and nano-devices and high-precision moulds (Fig. 4e). With their remarkable mechanical properties and corrosion and oxidation resistance, they can be used as micro-components such as gears for applications in harsh environments (Fig. 4f). With their high $T_g$, oxidation resistance and mechanical properties, combined with inexpensive and versatile processability by thermoplastic forming, they are in many ways superior to currently used Ir alloys, which have broad applications but suffer from poor processability owing to their intrinsic brittleness[31].

The development of high-temperature BMGs has taken nearly three decades so far[32,33]. However, previous trial-and-error approaches focusing on eutectic compositions (in particular, in tungsten-based alloys) have identified only glass formers that require very high cooling rates to avoid crystallization[32,33]. The discovery process described here for the Ir–Ni–Ta–(B) alloys represents a paradigm shift in the development of practical BMGs because it allows for the simultaneous optimization of many of the properties required for a BMG to be of commercial use.

## Online content

Any methods, additional references, Nature Research reporting summaries, source data, statements of data availability and associated accession codes are available at https://doi.org/10.1038/s41586-019-1145-z.

Received: 8 February 2018; Accepted: 13 February 2019;
Published online 1 May 2019.

1. Klement, W., Willens, R. H. & Duwez, P. Non-crystalline structure in solidified gold–silicon alloys. *Nature* **187**, 869–870 (1960).
2. Greer, A. L. Metallic glasses… on the threshold. *Mater. Today* **12**, 14–22 (2009).

3. Li, Y. L., Zhao, S. F., Liu, Y. H., Gong, P. & Schroers, J. How many bulk metallic glasses are there? *ACS Comb. Sci.* **19**, 687–693 (2017).
4. Tsai, P. & Flores, K. M. High-throughput discovery and characterization of multicomponent bulk metallic glass alloys. *Acta Mater.* **120**, 426–434 (2016).
5. Ma, D., Tan, H., Wang, D., Li, Y. & Ma, E. Strategy for pinpointing the best glass-forming alloys. *Appl. Phys. Lett.* **86**, 191906 (2005).
6. Deng, Y. P. et al. A combinatorial thin film sputtering approach for synthesizing and characterizing ternary ZrCuAl metallic glasses. *Intermetallics* **15**, 1208–1216 (2007).
7. Ding, S. Y. et al. Combinatorial development of bulk metallic glasses. *Nat. Mater.* **13**, 494–500 (2014).
8. Li, Y., Guo, Q., Kalb, J. A. & Thompson, C. V. Matching glass-forming ability with the density of the amorphous phase. *Science* **322**, 1816–1819 (2008).
9. Chen, G. et al. Polysynthetic twinned TiAl single crystals for high-temperature applications. *Nat. Mater.* **15**, 876–881 (2016).
10. Inoue, A., Shen, B. L., Koshiba, H., Kato, H. & Yavari, A. R. Cobalt-based bulk glassy alloy with ultrahigh strength and soft magnetic properties. *Nat. Mater.* **2**, 661–663 (2003).
11. Senkov, O. N., Wilks, G. B., Scott, J. M. & Miracle, D. B. Mechanical properties of $Nb_{25}Mo_{25}Ta_{25}W_{25}$ and $V_{20}Nb_{20}Mo_{20}Ta_{20}W_{20}$ refractory high entropy alloys. *Intermetallics* **19**, 698–706 (2011).
12. Inoue, A. Stabilization of metallic supercooled liquid and bulk amorphous alloys. *Acta Mater.* **48**, 279–306 (2000).
13. Miracle, D. B. & Senkov, O. N. A critical review of high entropy alloys and related concepts. *Acta Mater.* **122**, 448–511 (2017).
14. Schroers, J. On the formability of bulk metallic glass in its supercooled liquid state. *Acta Mater.* **56**, 471–478 (2008).
15. Nagel, S. R. & Tauc, J. Nearly-free-electron approach to theory of metallic glass alloys. *Phys. Rev. Lett.* **35**, 380–383 (1975).
16. Yu, H. B., Wang, W. H. & Bai, H. Y. An electronic structure perspective on glass-forming ability in metallic glasses. *Appl. Phys. Lett.* **96**, 081902 (2010).
17. Wang, L. F., Zhang, Q. D., Cui, X. & Zu, F. Q. An empirical criterion for predicting the glass-forming ability of amorphous alloys based on electrical transport properties. *J. Non-Cryst. Solids* **419**, 51–57 (2015).
18. Liu, Y. H. et al. Thermodynamic origins of shear band formation and the universal scaling law of metallic glass strength. *Phys. Rev. Lett.* **103**, 065504 (2009).
19. Ma, D. et al. Elastic moduli inheritance and the weakest link in bulk metallic glasses. *Phys. Rev. Lett.* **108**, 085501 (2012).
20. Cao, C. R. et al. Correlation between glass transition temperature and melting temperature in metallic glasses. *Mater. Des.* **60**, 576–579 (2014).
21. Collver, M. M. & Hammond, R. H. Stability of amorphous transition-metal films. *J. Appl. Phys.* **49**, 2420–2422 (1978).
22. Wang, Y. M., Wang, Q., Zhao, J. J. & Dong, C. Ni–Ta binary bulk metallic glasses. *Scr. Mater.* **63**, 178–180 (2010).
23. Johnson, W. L. Bulk glass-forming metallic alloys: science and technology. *MRS Bull.* **24**, 42–56 (1999).
24. Hao, G. J., Lin, J. P., Zhang, Y., Chen, G. L. & Lu, Z. P. Ti–Zr–Be ternary bulk metallic glasses correlated with binary eutectic clusters. *Mater. Sci. Eng. A* **527**, 6248–6250 (2010).
25. Bernard, V. B., Kuprina, V. V. & Burnasheva, V. V. Iridium–nickel–tantalum ternary alloy phase diagram *ASM Alloy Phase Diagrams Database* (ed. Villars, P.) (ASM International, Russel Township, 2016).
26. Liu, Y. H., Fujita, T., Aji, D. P. B., Matsuura, M. & Chen, M. W. Structural origins of Johari–Goldstein relaxation in a metallic glass. *Nat. Commun.* **5**, 3238 (2014).
27. Turnbull, D. Under what conditions can a glass be formed? *Contemp. Phys.* **10**, 473–488 (1969).
28. Lu, Z. P. & Liu, C. T. Glass formation criterion for various glass-forming systems. *Phys. Rev. Lett.* **91**, 115505 (2003).
29. Kumar, G., Neibecker, P., Liu, Y. H. & Schroers, J. Critical fictive temperature for plasticity in metallic glasses. *Nat. Commun.* **4**, 1536 (2013); corrigendum **4**, 2357 (2013).
30. Gangopadhyay, A. K. et al. Correlation of the fragility of metallic liquids with the high temperature structure, volume, and cohesive energy. *J. Chem. Phys.* **146**, 154506 (2017).
31. Ohriner, E. K. Processing of iridium and iridium alloys: methods from purification to fabrication. *Platin. Met. Rev.* **52**, 186–197 (2008).
32. Rohr, L., Reimann, P., Richmond, T. & Guntherodt, H. J. Refractory metallic glasses. *Mater. Sci. Eng. A* **133**, 715–717 (1991).
33. Yoshimoto, R., Nogi, Y., Tamura, R. & Takeuchi, S. Fabrication of refractory metal based metallic glasses. *Mater. Sci. Eng. A* **449–451**, 260–263 (2007).


**Acknowledgements** We thank D. Q. Zhao and D. W. Ding for experimental assistance. This work was partly supported by the National Key Research and Development programme of China (grant number 2017YFB0701900), the MOST 973 programme (grant number 2015CB856800), the NSF of China (grant numbers 11790291 and 61888102), the Key Research programme of Frontier Sciences of the Chinese Academy of Sciences (grant number QYZDY-SSW-JSC017) and the Strategic Priority Research programme of the Chinese Academy of Sciences (grant number XDB30000000). J.S. is grateful for support by NSF DMR through award number 1609391 for the combinatorial fabrication and XRD mapping. Y.H.L. acknowledges funding from the National Science Fund for Distinguished Young Scholars of the NSF of China (grant number 51825104), the Hundred Talents programme of the Chinese Academy of Sciences and the National Thousand Young Talents programme of China.

**Reviewer information** *Nature* thanks Chain Tsuan Liu and the other anonymous reviewer(s) for their contribution to the peer review of this work.

**Author contributions** Y.H.L. conceived and led the research. Y.H.L., J.S. and W.-H.W. supervised the project. Y.H.L. and M.-X.L. designed the experiments (with advice from P.W., H.-Y.B., M.W.C., J.S. and W.-H.W.). M.-X.L. conducted the experiments. S.-F.Z. and J.S. carried out combinatorial fabrication, XRD mapping and bending tests. Z.L., A.H. and M.W.C. conducted nanoindentation tests. M.-X.L. and Y.H.L. wrote the manuscript with input and comments from all authors.

**Competing interests** The authors declare no competing interests.

**Additional information**

**Extended data** is available for this paper at https://doi.org/10.1038/s41586-019-1145-z.



**Correspondence and requests for materials** should be addressed to Y.L.

## METHODS

**Sample preparation.** The combinatorial thin-film libraries were fabricated by magnetron co-sputtering deposition from elemental sputtering targets, and 100-mm-diameter Si wafers were used as substrates[6]. Alloy ingots were prepared by arc melting in Ar atmosphere. Copper-mould suction casting was used to fabricate rod samples. Micro-wires were fabricated by rapidly heating 1-mm-diameter glassy rods into the supercooled liquid region, followed by rapid drawing out (by attaching a weight to one end of the rod).

**Compositional and structural characterizations.** The compositions of the combinatorial libraries, calibrated with bulk alloys of known compositions, were measured by energy-dispersive X-ray spectroscopy attached to a Phenom scanning electron microscope. X-ray diffraction was used to characterize phase formation of the combinatorial libraries by using Rigaku SmartLab X-ray diffractometer with a Cu-K$\alpha$ radiation source[6]. The amorphous nature of rod samples was confirmed by XRD using a Bruker D8 X-ray diffractometer with a Cu-K$\alpha$ radiation source.

**Electrical resistance measurement and its correlation with glass forming ability.** Sheet resistance mapping over the as-deposited films was done using the automatic four-point probes method (Cresbox, Napson). For each wafer, 225 uniformly distributed points were measured. The argument of Nagel and Tauc[15] assumed a spherical Fermi surface and a spherically symmetric structural factor in an amorphous structure. Because glass, considered as a liquid metal, is in a metastable state and any perturbation due to a decreased degree of disorder will destroy the spherical symmetry of $S(q)$, the total energy of the system increases as more electron states are moved up to the Fermi energy $E_F$, where they have higher energy. According to Nagel and Tauc[15], the increased stability of an amorphous structure is realized when the Fermi surface touches the quasi-Brillouin boundary, or $q_p = 2K_F$ (where $K_F$ is the Fermi wave vector, and $q_p$ is the first maximum of the structural factor $S(q)$). Energy gaps are predicted to occur at the boundaries of Brillouin zones, at which energy levels are forbidden and the density of energy states is suppressed, leading to reduced electronic conductivity[16]. In the Nagel–Tauc model[15], transition metals as well as the noble metals are treated as if they had only one free electron per atom in the liquid, and the effect of alloying is treated as a rigid shift of $E_F$ and $K_p$. These two assumptions were verified by Nagel and Tauc with experimental data[15]. Recent reports on various transition-metal systems further indicate a positive correlation between glass-forming ability and electronic resistivity[15,16]. Here we took this correlation as a guideline and carried out resistivity mapping to narrow down the composition range in which alloys of high glass-forming ability may exist.

**Thermal analysis.** The differential scanning calorimetry experiments were performed using a DSC 404F3 (Netzsch) under a constant flow of high-purity argon gas. The heating rate was 0.33 K $s^{-1}$. Thermal mechanical analysis at a heating rate of 0.083 K $s^{-1}$ under a constant flow of high-purity argon gas was conducted by using a TMA 402F3 (Netzsch). The load applied on the specimen was 3 gram force.

**Mechanical characterization.** Compressive tests were conducted on 1 mm diameter × 2 mm long rod samples by using a custom-made high-temperature mechanical tester at a strain rate of 0.012 $s^{-1}$. The bending strain to failure rate was measured by bending beams (10 mm × 2 mm × 0.85 mm) around mandrels of different radii at room temperature. Hardness and elastic modulus were measured using nanoindentation equipped with a standard Berkovich indenter.

**Oxidation behaviour.** Weight loss measurements were performed in air in a Mettler TGA/SDTA851e Instrument. Cylinder specimens 2 mm in diameter and 1 mm in length were scanned from 323 K to 1,473 K at a constant heating rate of 0.33 K $s^{-1}$. Furthermore, we annealed $Ir_{33}Ni_{28}Ta_{39}$ BMG disks in air at different temperatures (600 K, 700 K, 800 K and 1,000 K). XRD characterizations on the surface of the annealed disks indicated that the oxide layer is mainly composed of $Ta_2O_5$ and NiO. $Ta_2O_5$ starts to form at 800 K, while NiO starts to form at 1,000 K (Extended Data Fig. 1). We also conducted characterizations on the cross-section of the annealed disk by scanning electron microscopy, as shown in Extended Data Fig. 2. Composition mapping by energy-dispersive X-ray spectroscopy indicates that the thickness of the oxide layer is about 4 μm after the disks were annealed at 1,000 K for 1 min, because beyond the 4-μm-thick oxide layer, the concentrations of Ir, Ta, and Ni change back to their nominal ratio and that of O decays to zero. After being annealed for 60 min at 1,000 K, the thickness of the oxide layer increased from 4 μm only to 8 μm. A clear boundary of oxide layer can be seen (Extended Data Fig. 2). For the sample annealed for 1 min at 1,000 K, Ir and Ta decreased a little. After annealing for 60 min, Ir and Ta remained nearly constant, but Ni decreased substantially. This is probably owing to the formation of NiO, which is denser than $Ta_2O_5$ and can prevent further oxidation. Extended Data Fig. 2 also shows the microstructure of the oxide layer at different annealing times. With prolonged annealing time, no obvious change could be seen in the oxide layer, suggesting that the dense and uniform layer composed of $Ta_2O_5$ and NiO limited the oxide reaction to the surface.

**Impurity of the developed BMGs.** We analysed the impurities of $Ir_{33}Ni_{28}Ta_{39}$ BMG by using a LECO TC-600 nitrogen/oxygen analyser and an infrared absorption carbon–sulphur analyser. As shown in Extended Data Table 1, the contents of impurities, including oxygen, carbon and nitrogen, were all beyond the resolution of the analyser (0.01 at.%), indicating the low concentration of these impurities. We also analysed the impurities of the raw Ir, Ni, Ta materials. Again, the contents are all below 0.01 at.%.

## Data availability

The authors declare that the data supporting the findings of this study are included within the paper and available from the corresponding author on reasonable request.

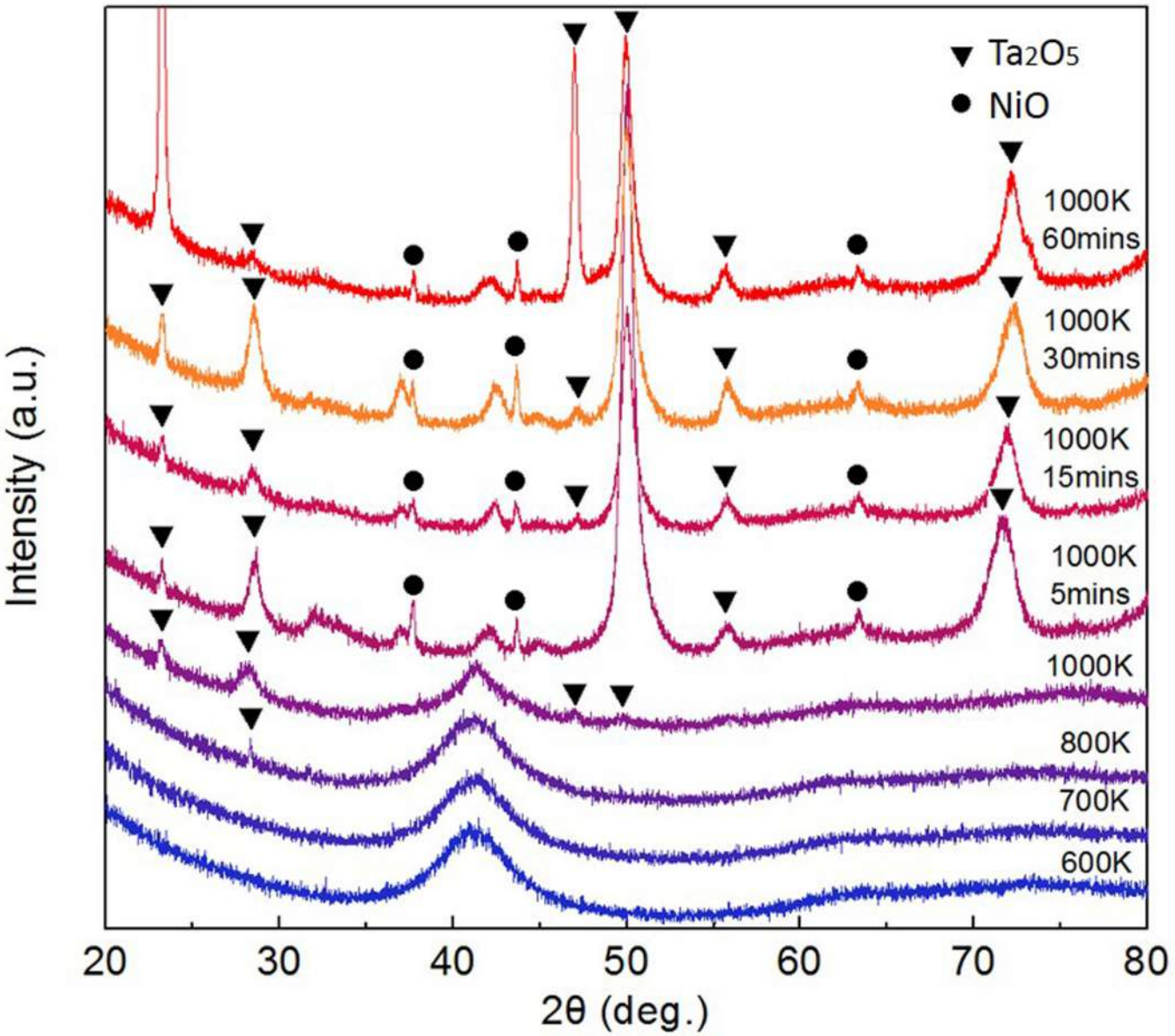


**Extended Data Fig. 1 | Oxide formation with temperature and time.** XRD characterizations on the surfaces of annealed BMG disks indicate that the oxide layer is mainly composed of $Ta_2O_5$ and NiO.

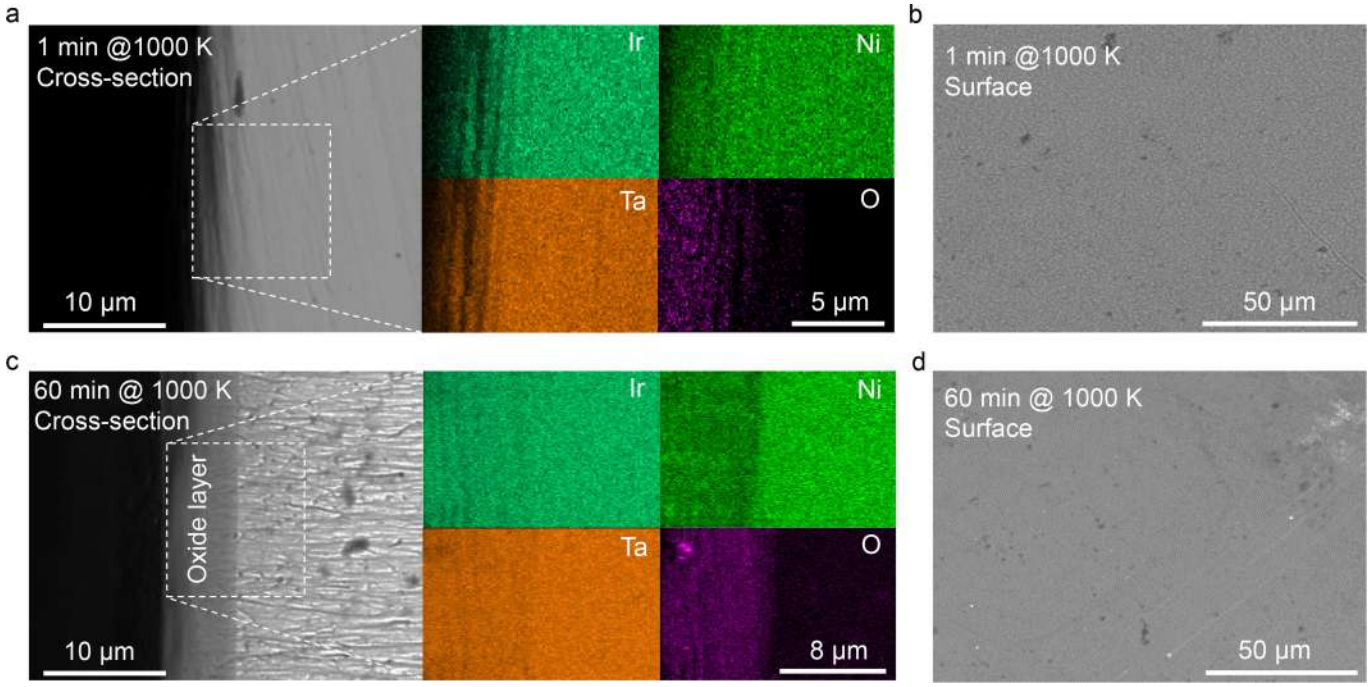


**Extended Data Fig. 2 | Morphologies of oxide layer. a**, **b**, Cross-section and surface morphology along with corresponding element distribution on disk sample annealed at 1,000 K for 1 min. **c**, **d**, Cross-section and surface morphology along with corresponding element distribution on disk sample annealed at 1,000 K for 60 min.

**Extended Data Table 1 | Concentration of impurities in the $Ir_{33}Ni_{28}Ta_{39}$ BMG**

| Element | O | C | N | Pb | Si | Ca | Se | Ag |
|---|---|---|---|---|---|---|---|---|
| Concentration | <0.01 % | <0.01 % | <0.01 % | 15 PPM | 10 PPM | 3 PPM | 3 PPM | 2 PPM |

PPM, parts per million.